Theor Chem Acc (2005) 114: 235–241
DOI 10.1007/s00214-005-0666-8

REGULAR ARTICLE

Nurbosyn U. Zhanpeisov · Masakazu Anpo

Theoretical ab initio study of the intrinsic band gap in semiconductor oxides based on modified titanium dioxides

Received: 8 July 2004 / Accepted: 1 September 2004 / Published online: 17 June 2005

Abstract The results of Hartree–Fock calculations mimicking the effect of transition metal ions on electronic and structural properties of rutile and anatase structures have been presented. The vertical excitation energies of modified structures were estimated by performing single point configuration interaction calculations including only singlets (CIS). The main discussion concerns the excitation shifts into a longer wavelengths region and their relation to the frontier orbitals responsible for the observed band gap changes. The results obtained allow us to give some insight into understanding the target phenomenon as well as point out on the importance of boundary frontier orbitals. Particularly, it was shown that the transition metal modified anatase structures prepared by modern ion-engineering techniques are superior compared to those prepared by the use of conventional ones.

1 Introduction

Recently, an application of photocatalysts for the removal of pollutant NO and other nitrogen oxides become one of the promising strategies for environmental pollution control [1]. This is because these photocatalysts are environmentally harmonious and friendly as well as clean. Among them, titanium dioxide, either as rutile or anatase, has some evident advantages because of its relatively inexpensive prices, non-toxicity, high thermal stability, etc. Due to reliable surface areas and/or relatively low band gap values, these materials can be used either as reservoirs to adsorb molecules or as visible light. However, the most widely applied titanium dioxide photocatalyst can only absorb to itself about 3–5% of the solar beams reaching the Earth, leaving an enormous part of the solar energy without its effective use. Thus, attempts to increase the above threshold as well as to extend the photoactivity of titania-based catalysts to cover the range of visible light in order to utilize solar energy more efficiently are highly attractive and important.

Some research works that appeared in the literature are devoted to the application of substitutional doping treatments of the titania with non-metal atoms such as carbon, sulfur, and nitrogen that create non-metal defect sites within the parent photocatalyst [2–4]. In the recent work of Diwald et al. [5], the incorporation of nitrogen monoanions into TiO_2 single crystals was achieved by sputtering with N_2^+/Ar^+ mixtures and subsequent annealing to 900 K under ultrahigh vacuum conditions. The catalyst thus modified exhibited an unexpected blue shift in the O_2 photodesorption compared to undoped crystals of titania. As has been noted elsewhere [6], the incorporation of non-metals into the lattice structure of titania is just one of the possible ways to decrease the desired band gap value for the target titania catalyst. For example, there might be another way of a modification of the parent photocatalyst via doping with transition metal containing compound, either through a conventional ion-exchange technique or advanced ion-engineering methods [7–10]. The latter metal-ion-implantation techniques can be expected to be superior in preparing photocatalysts based on powdered titanium dioxide that may operate under visible light irradiation. It is believed that the surrounding of the impurity cation within the parent oxide would then play a decisive role in the decrease of the estimated band gap. A particular case of this modification corresponds to a treatment of the photocatalyst with alkaline metal [6, 11–14]. In the latter case, alkaline metal is expected to be involved in the reduction processes of Ti^{4+} to Ti^{3+}, thus opening a way for a decrease in the band gap [6].

The present study discusses the results of ab initio Hartree–Fock calculations obtained for the transition metal modified rutile and anatase structures while using a well-known cluster approach. The respective vertical excitation energies were estimated by performing a single point configuration

N.U. Zhanpeisov · M. Anpo
Department of Applied Chemistry,
Osaka Prefecture University,
1-1 Gakuen-cho, Sakai, Osaka 599-8531, Japan

Present address: N.U. Zhanpeisov (✉)
Department of Chemistry,
Graduate School of Science,
Tohoku University, Sendai 980-8578, Japan
Fax: +81-22-2176570
E-mail: nurbosyn@orgphys.chem.tohoku.ac.jp

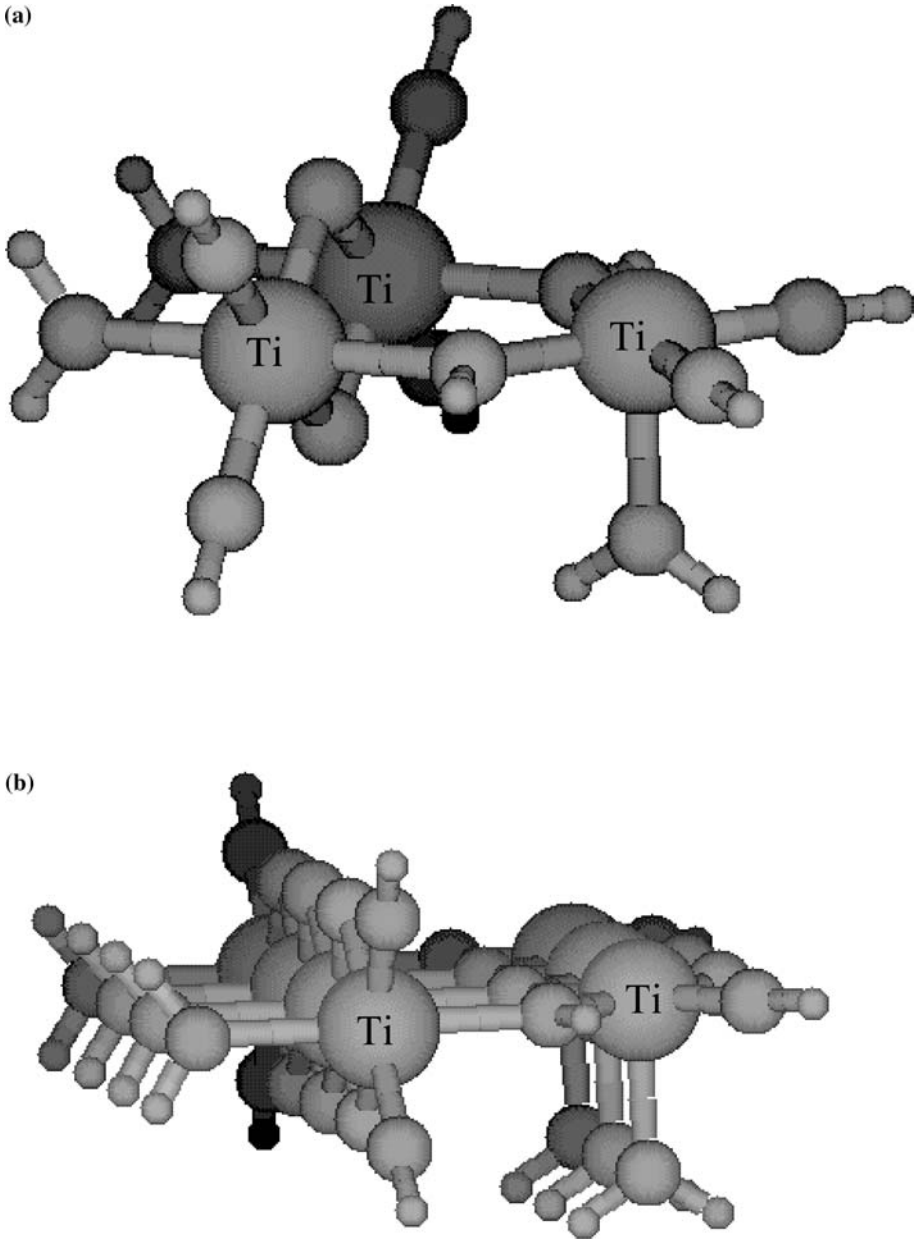

Fig. 1 The smallest (**a**) and extended (**b**) cluster models mimicking (110) plane of rutile structures

interaction calculations including only singlets (CIS), while in few cases, their adiabatic excitation energies are also estimated. The results obtained are expected to give some insight in understanding the target phenomenon.

The paper is organized as follows. Section 2 outlines the computational details and cluster models applied. Section 3 presents the geometric structures and relative energetic and molecular properties of rutile and anatase that are modified by doping of transition metal ions. Finally, Sect. 4 outlines the summary and conclusions.

2 Method of calculation and cluster models

Ab initio molecular orbital calculations were performed using the Gaussian 94 and Gaussian 98 program packages [15]. Precursor titanium dioxide as a rutile was modeled either by the edge-shared dititanium containing dioctahedra surrounded by five-fold coordinated titanium oxide or by an extended cluster model shown in Fig. 1 (denoted as models I and II, respectively) [16, 17]. Note that the extended model II is desired when one is interested in finding the most optimal

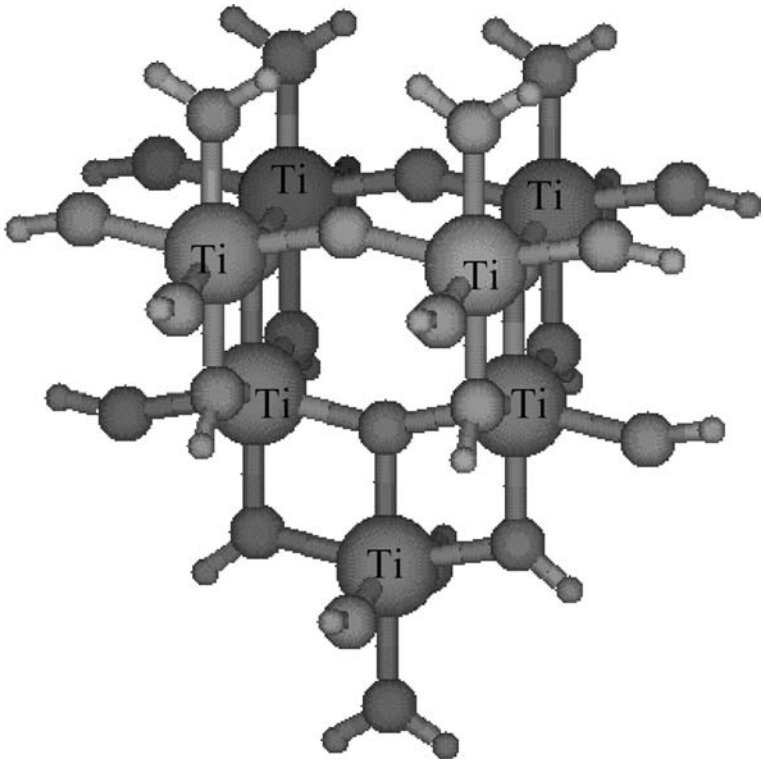

Fig. 2 Cluster model mimicking an anatase structure

active sites to stabilize an impurity Na atom on rutile modified with metal Na [6]. Thus, the former model I was mainly used to mimic the effects of transition metal ions within rutile structures. The latter were modeled via an isomorphous substitution of one of the sixfold coordinated Ti_{6c}^{4+} by desired transition metal cations. The most active anatase form of titanium dioxide was mimicked by the cluster model depicted in Fig. 2 (denoted as model III) that has also been used to describe the effects of impurity transition metal ions.

Since cutting substructures from titanium dioxide generates dangling bonds, they have been saturated with hydrogen atoms to avoid boundary effects and form terminal OH groups or water molecules, respectively. In such a sense, the final cluster models satisfy for the stoichiometry, boundary conditions, and electroneutrality [17,18].

Geometry optimizations were carried out at the Hartree–Fock (HF) level of theory using the standard double zeta quality Lanl2dz basis set. Both rutile structures mimicking (110) surfaces were fully optimized while for anatase, the geometry was fixed at experimental values [19]. In addition, geometries of the above rutile structures were optimized also at the HF level of theory using the standard 6-31G* basis set.

To estimate the vertical excitation energies, we performed calculations on excited states using single excitation CI (configuration interactions). Since adiabatic excitation energies are known to be much smaller than those of vertical excitation ones [18], a few additional calculations were performed to estimate adiabatic excitation energies. Evidently, the excited state geometries for the latter are expected to be different than those found for the ground states.

3 Results and discussion

3.1 Preliminary remarks

As has been shown elsewhere [6], the applied level of the theory is well justified if one interests on the reactivity, structural, energetic, and electronic properties of representative oxide systems. For example, the HF/Lanl2dz level leads to qualitatively similar descriptions of properties of metal oxide catalysts (silica, alumina-silica, zeolites, Ti-silicalite, etc.) to those obtained at the popular density functional theory level (either B3LYP/Lanl2dz or B3LYP/6-31G*). Although both levels of calculations complement each other, the latter DFT calculations result in relatively longer bond distances and in much less-opened bond angles (if the optimized geometry is concerned) than those obtained at the HF level [6,20]. For Ti-silicalites with an implanted V ion, both levels of theories show that the V=O group occupies the trans-position as regard to the surface Ti–OH group [20]. However, the difference between the cis- and trans-orientations is rather small

Table 1 The estimated properties (LUMO-HOMO energy difference, Δ (au); LUMO (au); Mulliken charge on Ti_{6c}, an impurity metal (Me) and O atoms (Q, all e^-); spin density on impurity metal atom (ρ, au); /S^2/ parameter before and after spin annihilation) of pure and modified rutile catalysts as calculated at the UHF/Lanl2dz level

	Δ	LUMO	Q_{Ti}	Q_{Me}	Q_O^a	ρ	/S^2/$_{in.}$	/S^2/$_f$
Rutile	0.37467	0.02303	2.03		−0.97			
V^{4+}/rut	0.37269	0.02409	2.00	1.88	−0.92	1.11	0.7794	0.7506
Cr^{4+}/rut	0.33102	0.02586	1.92	1.42	−0.88	0.95	2.0147	2.0001
Cr^{4+}/rut	0.36722	0.02434	1.96	1.65	−0.80			
Fe^{4+}/rut	0.34676	0.02231	1.97	1.60	−0.71	2.93	6.9005	6.0968
Fe^{4+}/rut	0.35659	0.02276	1.98	1.50	−0.73	1.79	2.0384	2.0006
Fe^{4+}/rut	0.34320	0.02327	1.98	1.46	−0.70			
Ni^{4+}/rut	0.25160	0.02673	1.60	1.19	−0.64	1.80	12.031	12.000
Mn^{4+}/rut	0.33739	0.02256	1.96	1.54	−0.51	1.92	4.4081	3.7638
Co^{4+}/rut	0.25884	0.00574	1.94	1.20	−0.63	−0.98	5.3652	4.7643

[a]Protruded bridging O_{br} site

Table 2 CIS//HF/Lanl2dz calculations results (LUMO–HOMO energy difference (Δ, au), LUMO (au), Mulliken charges on distinct atomic site (all e^-), the first three single excitation energies (E, eV) (band lengths, nm)) of various modified rutile structures at the first excited singlet state geometry of rutile

	Δ	LUMO	Q_{Ti}	Q_O^{br}	Q_{Me}	E_1	E_2	E_3
Rutile	0.36017	0.01959	2.04	−1.01		4.46 (278)	4.88 (254)	5.21 (238)
V^{4+}/rut	0.35406	0.02019	2.02	−0.92	1.89	2.83 (437)	4.08 (304)	4.46 (278)
Cr^{4+}/rut	0.30143	0.01010	1.76	−0.86	1.57	2.63 (472)	3.46 (358)	–
Fe^{4+}/rut	0.35351	−0.0048	2.01	−0.73	1.57	3.39 (365)	3.74 (331)	–
Zr^{4+}/rut	0.35022	0.01851	1.90	−1.04	2.32	4.45 (279)	4.87 (254)	5.20 (238)
Hf^{4+}/rut	0.34805	0.01825	1.89	−1.04	2.35	4.44 (279)	4.87 (255)	5.19 (239)
Si^{4+}/rut	0.35427	0.02019	1.97	−1.04	2.38	4.45 (279)	4.88 (254)	5.21 (238)
Ge^{4+}/rut	0.35212	0.01987	2.01	−1.03	2.27	4.44 (279)	4.88 (254)	5.21 (238)
Sn^{4+}/rut	0.34441	0.01804	1.99	−1.10	2.52	4.42 (280)	4.87 (255)	5.19 (239)
Pb^{4+}/rut	0.34262	0.01857	1.99	−1.07	2.41	4.43 (280)	4.87 (255)	5.19 (239)
V^{5+}/rut	0.32516	−0.00912	2.01	−0.96	1.62	3.94 (315)	4.69 (264)	5.23 (237)
Cr^{3+}/rut	0.33980	0.02189	2.04	−1.07	1.66	–	4.51 (275)	4.83 (256)

showing that the vanadyl V=O group on these materials can be freely rotated around the V–O–Ti linkage.

Another observation is that the vertical excitation energies (at the CIS level) estimated for the representatives of silica, Ti-silicalite, and V-doped Ti-silicalite models containing one surface OH-group associated with the central T atom in 5T cluster models, where T = Si or Ti, describe well their relative reactivity order as well as the changes that take place in the frontier orbitals [20]. For example, the vertical excitation energy value for the silica is quite large and is accompanied by very low intensity. In going from silica to Ti-silicalite and further to V-doped Ti-silicalite, the excitation energy value gradually decreases, showing that the excitation shifts into longer wavelengths region. The order of such changes correlates well either with the LUMO level energy or with the difference in the LUMO and HOMO energies (Δ) estimated for these models: the lower the LUMO or the LUMO-HOMO band gap, the lower the vertical excitation energy [20]. The obtained correlation is important for further discussions on modified titanium dioxide catalysts. Moreover, these preliminary theoretical results support the experimental data found for silicalite derivatives [21], where the largest absorption band shifts with higher wavelengths are indeed observed for the V ion-implanted Ti-silicalite catalysts.

3.2 Transition metal modified rutile

The cluster model I is mainly used to study the effects of transition ion impurities on electronic structures of the modified rutile catalysts. We have first studied the isomorphous substitution of one of the sixfold coordinated Ti^{4+} by Me^{4+} where Me = V, Cr, Fe, Ni, Mn, Co, provided that the latter transition metal ions are in the same oxidation state as the precursor Ti site. This approximation is aimed to get some preliminary insight into how such substitutions would affect the border orbital energies, i.e., HOMO and LUMO energies. Although they do not directly answer for the changes in the vertical excitation energy levels in these modified catalysts (since they are not optimal for local orientations of impurity ions within the rutile structure), they could be expected to shed some light to further our discussion. The results obtained at the HF/Lanl2dz level are presented in Table 1. As is clear, the order of changes in the (LUMO–HOMO) energy difference is found to be as follows:

$$Ni^{4+} < Co^{4+} < Cr^{4+} < Mn^{4+} < Fe^{4+} < V^{4+} < Ti^{4+}$$

Accordingly, the Ni^{4+}- and Co^{4+}- containing rutile catalysts should be expected as the most effective and potential ones compared to those of V^{4+}- containing catalysts. However,

Table 3 CIS//HF/Lanl2dz calculations results (total energy (E_{tot}, au), LUMO-HOMO energy difference (Δ, au), LUMO energy (au), Mulliken charge on bridging O site (e^-), the first three excitation energies (E, eV) (band lengths, nm)) for the rutile and its V- and Cr- modified analogues

	$-E_{tot}$	Δ	LUMO	Q_O^{br}	μ	E_1	E_2	E_3
Rutile	1154.3855	0.37467	0.02303	−0.97	4.1	6.56 (189)	6.78 (183)	6.85 (181)
V^{5+}/rut	1166.7112	0.36997	0.02214	−0.88	5.3	3.15 (394)	3.96 (313)	–
V^{5+}/rut[a]	1166.7280	0.37037	0.01945	−0.91	5.9	3.58 (347)	4.16 (298)	4.32 (287)
rutile[b]	1154.3332	0.36017	0.01959	−1.01	4.7	4.46 (278)	4.88 (254)	5.21 (238)
Cr^{3+}/rut[c]	1182.9940	0.33467	0.02380	−1.06	4.8	5.31 (233)	5.89 (210)	–
Cr^{6+}/rut	1180.7855	0.31116	−0.01885	−0.90	4.9	3.63 (341)	4.01 (309)	4.15 (299)
Cr^{6+}/rut[d]	1180.7835	0.23136	−0.11355	−0.97	4.3			

[a]The V^{5+} next-nearest neighbor has been fully optimized
[b]At the first excited state geometry
[c]The proton added for charge neutrality is linked to the bridged O_{br} atom
[d]The fivefold coordinated Ti^{4+} is substituted by Cr^{6+}. This route is energetically less favorable by only 1.3 kcal/mol

this obtained order does not support the observed absorption band shifts [7,9,21,22] when going from rutile to those modified catalysts. At the same time, a strong spin contamination takes place for most of these modified catalysts. For example, in the case of Ni^{4+}/rutile, only about two of the total six unpaired electrons have been found to be located at the Ni site, while the rest have been delocalized on the Ti_{6c}, O_{br}, O_{t1} and O_{t2} atoms. They equal 0.85, 1.03, 1.05, and 1.06, respectively. The latter O_{br}, O_{t1}, and O_{t2} atoms relate to the bridging and two types of terminal oxygen atoms, respectively (see, Fig. 1). Note that all these three oxygen atoms have a bond with the impurity site and resemble its nearest-neighbor environment. A similar picture is also observed in the case of Cr^{4+}/rutile, in which only about half of the two unpaired electrons is localized on the Cr site while the other half is on the O_{t1} site linked to the Cr atom. In addition, such spin redistribution is the reason for an intrinsic instability in the modified catalysts thus obtained [9].

Next, we have optimized the first excited state geometry for the rutile structure at the CIS level. The optimized geometry thus obtained was then used to mimic the effects of impurity ions, mostly at the same oxidation state as the precursor Ti site, as well as of the V^{5+} and Cr^{3+}impurities. Table 2 shows calculation results of those various modified rutile structures. As is clear, the highest shifts in the absorption bands are observed for the Cr^{4+}- and V^{4+}- containing rutile structures, while a high spin contamination is still left for the former. At the same time, the observed shift can also be explained when one considers the replacement of Ti^{4+} by either V^{5+} or Cr^{3+}. The latter replacements can lead to the formation of more stable structures that are also more likely. The modification of the target rutile catalyst by implementing any other Me^{4+} from the IVA and IVB groups did not alter the estimated absorption bands as compared to the unmodified rutile. Note that for heavy impurity elements like Hf, there is no difference in the calculated adsorption bands, probably, because of the use of effective core potentials including also all these impurity cations.

Based on these results, a special attention is paid to the V- and Cr- modified rutile catalysts. It was suggested that within those modified catalysts, both the V and Cr can be favored to be in their optimal oxidation states, i.e., as V^{5+}, Cr^{3+}, and Cr^{6+}. The charge imbalance resulted by the replacement of these metals with different oxidation states were further adjusted through adding proton(s) to or removing proton(s) from the initial cluster model I. In addition, the optimal bond lengths for the Cr = O and V = O double bonds were either adjusted to those obtained from the respective four-fold coordinated small cluster models or fully optimized to get minimum energy environment for those impurities. As a consequence, the optimized structure for the V^{5+}/rutile were used to estimate the extent of the effect compared to that of the non-optimized one within the rutile structure. Evidently, the latter would estimate only qualitatively the changes that occurred within these materials; however, adiabatic excitation energy estimation would be good enough to compare it with the observed one. Table 3 lists the results of calculations for rutile and its V- and Cr-modified derivatives. In going from the rutile to the V- and further to Cr-containing rutile structures, the HOMO-level energy increases, which indirectly explains the band gap decrease during such modification. Introducing Cr^{3+} into the rutile structure causes the highest change both in the HOMO and in next-HOMO (not shown). Evidently, this latter change is due to the fact that the stoichiometry and charge balance need the presence of an extra additional H atom in the case of a modified Cr^{3+}/rutile cluster model. As a result, it leads to the formation of an open-shell structure and increases the HOMO energy level. We have further performed CIS calculations that model these V-doped and non-doped rutile structures. As can be expected, the vertical excitation energies have been calculated to be substantially larger since they originate from the non-optimal orientation of the constituent atoms at excited states that is based on the ground state geometries. However, the corresponding value of the excitation energy for the V-doped rutile has been estimated to be significantly lower than that of non-doped rutile. The respective adiabatic excitation energies have also been estimated. At the excited state geometry, all the Ti–O bonds are sufficiently elongated compared to those of the ground state. Moreover, the excitation energy for the V-doped rutile was found to be 68.7 kcal/mol lower than that of the non-doped rutile. Note that this finding is also within the experimental estimations both for titanium dioxides and Ti-silicalites containing V impurities.

Table 4 Properties (total energy (E_{tot}, au), multiplicity M, LUMO–HOMO energy difference (Δ, au), LUMO energy (au), Mulliken charges on distinct sites (Q, e^-), spin density on an impurity metal (ρ_{Me}, au)) of anatase and its modified analogues as calculated by HF/Lanl2dz level

	$-E_{tot}$	M	Δ	LUMO	Q_{Ti}	Q_{Me}	ρ_{Me}
Anatase	2516.3612	1	0.21639	−0.05543	2.36		
Cr^{3+}/anat	2544.9173	4	0.34870	0.01455	2.33	1.84	3.02
V^{5+}/anat	2528.6913	1	0.36556	0.00743	2.37	1.90	
Fe^{3+}/anat	2581.7653	6	0.30318	0.00674	2.01	1.43	3.86[a]
Fe^{4+}/anat	2581.3188	5	0.33131	−0.00066	2.32	1.81	4.66[b]
V^{4+}/anat	2529.4064	2	0.36426	0.00749	2.36	2.09	1.15
V^{5+}/anat[c]	2528.6829	1	0.15715	−0.10077	2.36	1.83	
Cr^{3+}/anat[d]	2544.9699	4	0.18109	−0.06306	2.36	1.83	3.04
Cr^{3+}/anat[e]	2544.8850	4	0.11648	−0.09404	2.34	1.89	3.01
Cr^{6+}/anat[f]	2542.7140	1	0.19790	−0.05913	2.36	1.55	

[a]High spin contamination is observed. There appear two unpaired electrons with a positive spin density on two bridging O_{br} sites (they are either exposed to the surface or to the bulk direction, respectively) as well as one unpaired electron on the Ti site linked through the bridging O_{br} site (exposed to bulk) with a negative spin density
[b]High spin contamination arises due to the appearance of a negative spin density on a bridging O_{br} site
[c]V^{5+} is in the deep bulk position
[d]The same as in (c). The extra proton is also located in the bulk
[e]The same as in (d) except that the extra proton is linked to the surface bridging O_{br} site. In both cases of (d) and (e), the border orbitals are originated from the orbitals of beta electrons
[f]Cr^{6+} is in the deep bulk position

Since the replacement of sixfold coordinated Ti^{4+} either by Cr^{3+}, Cr^{6+}, Fe^{2+} or Fe^{3+} leads to substantial lowering in the estimated band gap value for the initial rutile, one may expect that the excitation wavelengths would shift into higher values. However, one should take into account that when going from the rutile either to the Cr- or Fe-modified rutile structures, the stability (at least the thermal stability) of these materials decreases due to the imbalance in the ionic radii of those ions and that of the Ti^{4+} ion as well as due to high-spin contaminations originated by the presence of these impurity ions. Thus, vanadia-doped rutile would be expected to be the most effective catalyst for this reason.

3.3 Transition metal modified anatase

Model III shown in Fig. 2 contains four and one Ti^{4+}_{6c} that are the next-nearest atoms to the surface and to the deep bulk of anatase structure, respectively. As in the case of rutile, one of the Ti^{4+}_{6c}, either in the surface or bulk positions mentioned above, were isomorphously replaced with some other transition metal cation. Table 4 lists the results of calculations thus obtained. As is evident, not all replacements can explain the observed absorption band edge shifts into longer wavelengths. For example, the replacement of Ti^{4+} by transition metal cation that is near the surface layer of anatase leads to an increase in the (LUMO–HOMO) energy difference or to a decrease in HOMO-level energy as compared to that of pure anatase. This may also explain that the conventional ion-exchange methods used to obtain transition metal modified catalysts may not always result in obtaining more active modified anatase catalysts. Only in the cases when Ti^{4+} at the deep bulk position is replaced by impurity cation, one may observe substantial decrease in the (LUMO–HOMO) energy differences, thus indirectly explaining the desired absorption band edge shift into longer wavelength regions. Accordingly, the order of changes is as follows:

$$V^{5+}/\text{anatase} > Cr^{3+}/\text{anatase} > Cr^{6+}/\text{anatase} > \text{anatase}$$

This order is also applicable to modified rutile structures. At the same time, it explains the higher reactivity of anatase than rutile. Introducing the Cr^{3+} cation into the deep lattice positions of anatase structure leads to the highest change in both the HOMO and next-HOMO. Probably, this is due to the presence of charge-balancing extra proton in the modified Cr^{3+}/anatase cluster model. In Cr^{3+}/anatase, the new bridging OH-group is formed which, in turn, will establish two H-bonds with the next-nearest-neighbor two O sites. Thus, an open-shell structure formed increases the singly occupied HOMO-level energy to a substantial extent. Also, the additional proton prefers to be located in the deep bulk than at the bridging surface O site. All these findings show that the transition metal modified anatase structures prepared by modern ion-engineering techniques are superior compared to the conventional ones.

4 Conclusions

The results obtained in this study can be summarized as follows: for both anatase and rutile, an implementation of transition metal ions leads to a shift in the excitation into a longer wavelengths region. The order of changes in excitation as well as in activity can be represented in the following order:

$$V^{5+}/TiO_2 > Cr^{3+}/TiO_2 > Cr^{6+}/TiO_2 > TiO_2$$

However, to achieve the desired positive effect in the absorption band edge shifts into longer wavelength region, these transition metal ions should be incorporated into the deep bulk lattice positions as compared to those remaining near the surface layers. In the latter case, the results would be expected to be quite opposite since the (LUMO–HOMO) energy difference increases while the HOMO-level energy decreases substantially (or highly stabilized) for those modified catalysts.

This explains also the superiority of ion-implantation techniques over conventional ones.

References

1. Photofunctional zeolites: synthesis, characterization, photocatalytic reactions, light harvesting. Anpo M (ed) (2000) Nova Sci Publ, Huntington, New york
2. Khan SUM, Al-Shahry M, Ingler WB Jr (2002) Science 297:2243
3. Umebayashi T, Yamaki T, Itoh H, Asai K (2002) Appl Phys Lett 81:454
4. (a) Sato S (1986) Chem Phys Lett 123:126; (b) Asahi R, Morikawa T, Ohwaki T, Aoki K, Taga Y (2001) Science 293:269
5. Diwald O, Thompson TL, Goralski EG, Walck SD, Yates JT Jr (2004) J Phys Chem B 108:52
6. Zhanpeisov NU, Tsujimaru K, Anpo M (2004) Res Chem Intermed 30:107
7. Anpo M (1997) Catal Surv Jpn 1:169
8. Borgarello E, Kiwi J, Graetzel M, Pelizzetti E, Visca M (1982) J Am Chem Soc 104:2996
9. (a) Choi W, Termin A, Hoffmann MR (1994) J Phys Chem 98:13669; (b) Hoffmann MR, Martin ST, Choi W, Bahnemann DW (1995) Chem Rev 95:69
10. Klosek S, Raftery D (2001) J Phys Chem B 105:2815
11. Linsebigler AL, Lu G, Yates JT (1995) Chem Rev 95:735
12. See AK, Bartynski RA (1994) Phys Rev B 50:12064
13. Onishi H, Iwasawa Y (1996) Catal Lett 38:89
14. San Miguel MA, Calzado CJ, Sanz JF (2001) J Phys Chem B 105:1794
15. Frisch MJ, Trucks GW, Schlegel HB, Gill PMW, Johnson BG, Robb MA, Cheeseman JR, Keith T, Petersson GA, Montgomery JA, Raghavachari K, Al-Laham MA, Zakrzewski VG, Ortiz JV, Foresman JB, Cioslowski J, Stefanov BB, Nanayakkara A, Challacombe M, Peng CY, Ayala PY, Chen W, Wong MW, Andres JL, Replogle ES, Gomperts R, Martin RL, Fox DJ, Binkley JS, Defrees DJ, Baker J, Stewart JP, Head-Gordon M, Gonzalez C, Pople JA (1995) GAUSSIAN 94, Revision D.3, Gaussian Inc., Pittsburgh
16. Zhanpeisov NU, Matsuoka M, Yamashita H, Anpo M (1998) J Phys Chem B 102:6915
17. (a) Zhanpeisov NU, Higashimoto S, Anpo M (2001) Int J Quantum Chem 84:677; (b) Zhanpeisov NU (2004) Res Chem Intermed 30:133
18. (a) Zhidomirov GM, Kazansky VB (1986) Adv Catal 34:131 (b) Sauer J, Ugliengo P, Garrone E, Saunders VR (1986) Chem Rev 94:2095; (c) Zhanpeisov NU, Ju WS, Anpo M (2002) J Mol Struct (THEOCHEM) 592:155; (d) Zhanpeisov NU, Nakatsuji H, Hada M, Nakai H, Anpo M (1996) Catal Lett 42:173
19. Wyckoff RWG (1963) Crystal Structures Vol 1. Wiley, New York London
20. Zhanpeisov NU, Kanazawa Y, Yamashita H, Anpo M, Int J Quantum Chem 96:349
21. Zhanpeisov NU, Ikeue K, Takeuchi M, Kanazawa Y, Yamashita H, Anpo M (2002) In: Proc TOCAT4 Tokyo p 408
22. Yamashita H, Harada M, Misaka J, Takeuchi M, Ichihashi Y, Goto F, Ishida M, Sasaki T, Anpo M (2001) J Synchrotron Rad 8:569